Parameterization of Radiative Flux Profiles within Layer Clouds

HOWARD P. HANSON

Cooperative Institute for Research in Environmental Sciences, University of Colorado/NOAA, Boulder, CO 80309

VERNON E. DERR

NOAA Environmental Research Laboratories, Boulder, CO 80303

(Manuscript received 17 October 1985, in final form 15 April 1987)

ABSTRACT

The vertical structure of radiative flux profiles within clouds can have a significant impact on the thermodynamic processes that maintain and dissipate the clouds, particularly in the case of marine stratus and stratocumulus. However, dynamic models of these and other cloud systems have tended to include radiative transfer physics in only the most rudimentary fashion. This has caused potentially important feedback processes in the clouds to be neglected.

We present here simple formulations for the vertical structure of solar and infrared radiative fluxes within a layer cloud overlying a partially reflective surface. The parameterized profile shapes are analytic, with governing parameters derived from bulk radiative properties and more physically based radiative transfer models. The bulk cloud, subcloud layer and surface radiative properties are assumed to be known. The parameterizations are based on exponential functions of height, with decay scales related to cloud liquid water content. Although the results presented here are based on very simple assumptions about the cloud structure in the vertical, the method used is applicable to more general cases as well as to various other analytic and/or numerical radiative transfer calculations.

1. Introduction

Cloud processes have been a traditional focus of meteorology, but it is relatively recently that a role of clouds in climate, rather than weather (e.g., precipitation formation), has become of interest. Even more recent has been the treatment of clouds as interactive with the other processes in models of the climate. The main reason for this is undoubtedly the extremely small scales involved in cloud processes relative to those of climate dynamics: the description of the cloud field in a climate model must be limited to a very few variables at each grid point, if the cloud component is not to overwhelm the overall computation. Thus, the need for parametric models of clouds and cloud processes is indicated.

Among the most climatologically important cloud systems are the subtropical marine stratocumulus and stratus decks that occur off the west coasts of California, Peru, Angola and, to a lesser extent, Australia and Morocco (Schubert et al., 1979a; Hanson and Gruber, 1982). These cloud decks are highly reflective relative to the ocean and cover hundreds of thousands of square kilometers. Understanding the mechanics of these cloud systems has been advancing rapidly since Lilly's (1968) pioneering study; yet despite a large amount of literature in recent years there remain unanswered questions sufficient to initiate major field studies (Randall et al., 1984). One of the most important—and vexing—of questions concerns the roles of entrainment and radiation in the maintenance and dissipation of these clouds, and this will be a focus of the forthcoming FIRE (First International Satellite Cloud Climatology Project Regional Experiment) field research (Bretherton et al., 1983).

Although the effects of radiation on entrainment and cloud dissipation remain obscure, the inverse problem—the effects of clouds on radiation—has been studied extensively. Radiative transfer calculations with clouds included are complicated and time-consuming, but they have been successfully performed by a number of different investigators using various computational techniques (see, for example, the review by Stephens, 1984). The need for parametric representations of radiative fluxes for dynamical models has led to various parameterizations of cloud effects based on the detailed computations (e.g., Stephens, 1978b; Liou and Wittman, 1979). These parameterizations are designed to provide bulk cloud radiative properties (shortwave transmittance and reflectance; longwave emissivity) as functions of cloud properties (liquid water content and temperature) and of external factors such as solar zenith angle and surface albedo.

However, in order to understand the effects of radiation on clouds, it is not sufficient to use bulk properties alone, because the details of the radiation field within the clouds are important. That is, the *shape* of the radiative flux profile becomes crucial in under-

standing the clouds' behavior. This has been stressed most strongly in the stratocumulus modeling literature (Deardorff, 1976; Lilly and Schubert, 1980; Kahn and Businger, 1979; Randall, 1980b; Deardorff, 1981; Hanson and Gruber, 1982). Both detailed numerical calculations (Stephens, 1978a; Schmetz et al., 1981) and measurements (Stephens et al., 1978; Slingo et al., 1982a; Nicholls, 1984) of in-cloud radiative fluxes and resultant heating rates have shown strongly nonlinear distributions with height. Net solar flux distributions decrease monotonically with height below cloud top (e.g., Nicholls, 1984, Fig. 8), while net infrared (IR) fluxes decrease toward zero from the cloud-edge values (e.g., Slingo et al., 1982a, Figs. 3, 7, 11).

In this paper, we develop expressions to characterize this relatively simple behavior using exponential functions of height. Although detailed radiative transfer models can be used in cloud dynamical models (Oliver et al., 1978; Fravalo et al., 1981) they are very time consuming and not entirely compatible with the limited degrees of freedom in a simple cloud model (Schubert et al., 1979). The parameterizations developed here represent a physically realistic middle ground between detailed numerical models and the very rudimentary approach that has been used in much of the stratocumulus modeling literature.

We stress that the parameterizations developed here are meant to apply to relatively thin, horizontally homogenous layer clouds for which plane-parallel solutions to the radiative transfer equation are good approximations. This is obviously the first-order approach to radiative transfer in actual cloud systems, and investigations of inhomogenous cloud systems will need to include additional radiative transfer physics. An initial attempt to characterize the bulk radiative properties of inhomogenous layer clouds has been made by Welch and Wielicki (1985). Characterizing the *internal* radiative flux distribution in inhomogenous clouds will be a far more difficult problem. However, use of even the first-order approach developed here in a cloud dynamical model (Hanson, 1987) suggests that the internal radiative flux distributions are important to understanding layer cloud dynamics, particularly in dynamically active cloud systems such as stratocumulus.

2. Background

a. Cloud structure

The radiative-flux parameterization developed here requires specific assumptions to be made about the vertical structure of the cloud thermodynamic variables, particularly cloud liquid water. For maximum simplicity, we adopt a mixed layer formulation, in which thermodynamic quantities conservative for water phase changes are vertically constant (i.e., well-mixed) below cloud top. In this paper, the conservative quantities used are the total water mixing ratio, $r \equiv q + l$ where q and l are vapor (saturated in cloud) and liquid mixing ratios, respectively, and the liquid static energy [an analog of liquid potential temperature (Betts, 1975)] $s \equiv C_pT + gz - Ll$ where C_p, g and L are the specific heat of air at constant pressure, gravitational acceleration and the latent heat of condensation, respectively. The choice of liquid static energy is motivated by its close association with dry static energy, the analog of potential temperature (Hanson, 1987).

In thin cloud layers, the assumption that the total water mixing ratio r is constant with height implies, to first order, that both the vapor $q = q^*$ (saturated) and the liquid water l are linear with height. The total cloud liquid water content (LWC) is then

$$W = \int_{z_C}^{z_B} \rho(z) l(z)\, dz \approx \bar{\rho}\gamma_l \Delta z^2/2, \tag{2.1}$$

where $\bar{\rho}$ is an average air density, Δz the cloud thickness ($z_B - z_C$), and γ_l the increase of l with height. (Taking the various coefficients as constant and expressing Δz in m gives W g m^{-2} $\approx \Delta z^2/880$.) Since liquid static energy s is also constant, its definition and the linearity of l in z imply that the temperature T is linear in z with in-cloud gradient equal to a fraction of the adiabatic lapse rate (Hanson, 1984):

$$\gamma_T = -\beta g/C_p, \tag{2.2}$$

where

$$\beta = 1 - (L/g)\gamma_l. \tag{2.3}$$

The (nondimensional) thermodynamic quasi-constant β is discussed by Randall (1980a) and varies slightly about an average value of 0.5. In models that allow linear-in-z, in-cloud stratification of conservative variables (such as the trade cumulus models of Albrecht et al., 1979 and Rogers et al., 1985), the liquid water and temperature gradients remain constant, but differ from those given by an additive factor. Our method can therefore be easily applied to other types of layer clouds. Further, nonlinear vertical structures can also be accomodated, albeit with increased computational difficulty.

b. Parameterization method

In this paper, we are concerned primarily with the shapes of the vertical profiles of solar and IR radiative fluxes within layer clouds. This is because the radiatively induced heating and cooling, which depend on the derivative of these profiles, contribute to the clouds' heat budgets, and the positions of maxima and minima of heating and cooling within the clouds induce varying dynamic effects (Hanson, 1987). We are not so concerned with the absolute amounts of heating and cooling here. Therefore, to the extent possible, we nondimensionalize radiative-flux profiles and parameterize the profile shapes using results derived from more explicit radiative-transfer calculations.

For solar radiation, this method reduces simply to curve fitting, primarily because the sun is the only en-

ergy source. For IR radiation, matters are complicated by the fact that the surface, the atmosphere above the cloud and the cloud itself are all radiating bodies. We therefore adopt different approaches to parameterizing the two radiative bands.

Solar-flux profile shapes are parameterized by deriving decay scales from numerical radiative-transfer calculations using the ATRAD narrow-band model (Wiscombe et al., 1984). The decay scales are expressed in terms of W, the cloud LWC, and μ_0, the cosine of the solar zenith angle. The curve-fitting procedure produces solar flux profiles nearly identical to those from ATRAD.

Infrared-flux profile shapes are parameterized using the emissivity method. This can be accomplished analytically, and in so doing the large number of degrees of freedom due to the various IR energy sources (and their various strengths) can be handled. Using a numerical model for this purpose would require an extraordinary number of computations, and the economy of the analytic approach justifies its less explicit physics.

Sections 3 and 4 treat solar- and IR-flux profile shapes, respectively; F is used for solar fluxes and G for IR fluxes throughout, and the tilde is used consistently to designate the calculations with ATRAD and the emissivity method. Section 5 contains a summary and discussion. The completed parameterization is presented in appendix B.

3. Solar radiation

Our emphasis in this paper on the shapes of radiative-flux profiles does not imply that the absolute magnitudes of the fluxes are unimportant. For solar radiation, however, these can be found from the bulk cloud radiative properties, and the profiles can be nondimensionalized accordingly. In this analysis, we will assume that the bulk radiative properties are given.

For example, bulk cloud radiative properties have been parameterized for solar radiation by Stephens (1978b) and Liou and Wittman (1979). Differences between the two methods are illustrated in Fig. 1. In this figure, the gray "cloud" of data points represents an assemblage of several hundred observations under solid cloud cover of LWC and downward solar flux at the surface. The scatter is due to variations in surface albedo and to cases for which multiple cloud layers were present. The shape of this data cloud suggests that Stephens' (1978b; see also Stephens et al., 1984) two-band approach overpredicts the decrease in transmittance for small LWCs and underpredicts the transmittance for large LWCs. In contrast, the formulation of Liou and Wittman (1979) performs quite well at small LWC but breaks down for LWC greater than about 600 g m^{-2}, where their regressions begin to predict negative transmittances. In the cloud model used here, this is equivalent to a cloud about 725 m thick.

We assume that the following bulk properties are available: Ac, Rc, Tc, the absorptance, reflectance and transmittance of the cloud, respectively, and Rs, the surface albedo. These cloud values refer to the direct solar beam; the diffuse-beam values Acd, Rcd and Tcd are also needed if surface-cloud multiple reflections are to be included. Including these multiple reflections leads to the net cloud properties (Schneider and Dickinson, 1976)

$$\left.\begin{aligned} Ac_{\text{net}} &= Ac + AcdTcRs/R' \\ R_{\text{net}} &= Rc + TcRsTcd/R' \end{aligned}\right\} \tag{3.1}$$

for the net solar absorptance of the cloud and the net solar reflectance, respectively. In (3.1), the effect of multiple reflections is embodied in the factor $R' = 1 - RsRcd$. (The curves in Fig. 1 are the quantity Tc/R' for various surface albedos.)

The net solar fluxes at the cloud top (z_B) and the cloud base (z_C) are related to the bulk properties by

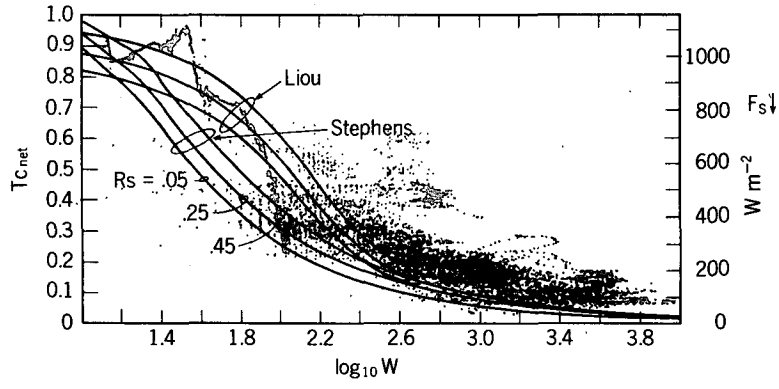

FIG. 1. Measured (data cloud) and calculated (curves) values of net cloud transmissivity for various surface albedos. Curves use Liou and Wittman's (1979) parameterization and Stephens et al.'s (1984) method. The data, taken with an Eppeley 0.3–2.8 μm pyranometer and microwave radiometer under solid clouds at various locations, are discussed in Derr and Hanson (1984).

$$\left.\begin{aligned} F_B &= -F_{B}\downarrow(1-R_{\text{net}}) \\ F_B - F_C &= -F_{B}\downarrow A c_{\text{net}} \end{aligned}\right\}, \tag{3.2}$$

where $F_B\downarrow$ is the downward solar flux just above the top of the cloud. These quantities can be used to nondimensionalize the solar-flux profile within the cloud by defining a function

$$\tilde{f}(\hat{z}) = [\tilde{F}_B - \tilde{F}(\hat{z})]/(\tilde{F}_B - \tilde{F}_C), \tag{3.3}$$

where $\hat{z} = (z - z_C)/(z_B - z_C)$ is a nondimensional height within the cloud layer. Our parameterization of the solar flux is thus reduced to deriving a function to fit $\tilde{f}(\hat{z})$. This is accomplished by fitting exponential functions to flux profiles computed with a numerical radiative transfer model.

For this purpose, we use the narrow-band numerical atmospheric radiative transfer model discussed in Wiscombe et al. (1984) and Wiscombe and Welch (1986). This model ("ATRAD") employs 290 wavebands over the interval 0.2–500 μm and includes Mie scattering by cloud drops and molecular absorption by all significant species in the atmosphere. The implementation of ATRAD used here divides the atmosphere from 0–50 km into 30 layers of varying thickness with 20 of those layers explicitly taken to be within the cloud layer. Stephens' (1978a) Sc-I cloud-drop distribution, which has an effective drop radius of 5.25 μm, was used, with droplet concentrations calculated to give liquid water mixing ratios identical to those implied by the mixed layer cloud model (2.1–2.3). Computations were made for ten cloud thicknesses, from 50–500 m, and five solar zenith angles, from 0°–80°.

The heavy curves in Figs. 2a and 2b show examples of $\tilde{f}$ from these ATRAD calculations. As expected, the normalized solar flux increases monotonically from zero at cloud top to unity at cloud base. The decay scale decreases with increasing cloud thickness (Fig. 2a) and, less strongly, with increasing solar zenith angle (Fig. 2b). The shapes of the curves in Fig. 2 are closely mimicked by the function

$$f(\hat{z}) = [1 - \exp(-(1-\hat{z})/\hat{\lambda}_s)]/[1 - \exp(-1/\hat{\lambda}_s)], \tag{3.4}$$

where $\hat{\lambda}_s$ is a nondimensional decay scale. The behavior of $\hat{\lambda}_s$ is illustrated in Figs. 3a and 3b. These values were found by regressing f vs $\tilde{f}$ (the nonlinear problem being solved iteratively). Note the nearly linear dependence of $\hat{\lambda}_s$ on μ_0 (Fig. 3b).

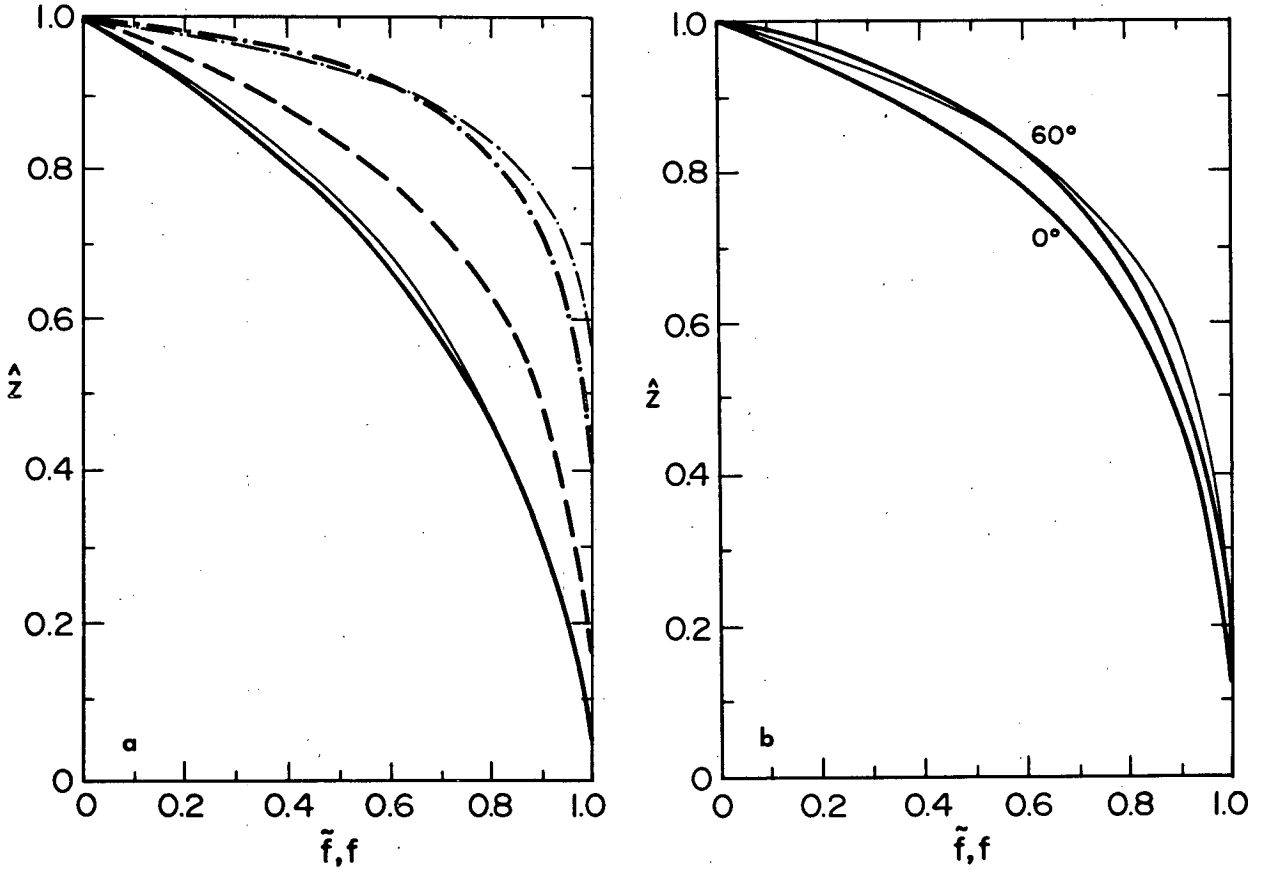

FIG. 2. Profiles of the nondimensional functions $\tilde{f}$ from ATRAD (heavy curves) and f from the parameterization (thin curves) vs nondimensional height for (a) different cloud thickness and (b) solar zenith angles. In (a), the cloud depths and LWCs are 100 m, 11.4 g m^{-2} (solid); 200 m, 45.5 g m^{-2} (dashed); and 500 m, 284 g m^{-2} (dash-dot).

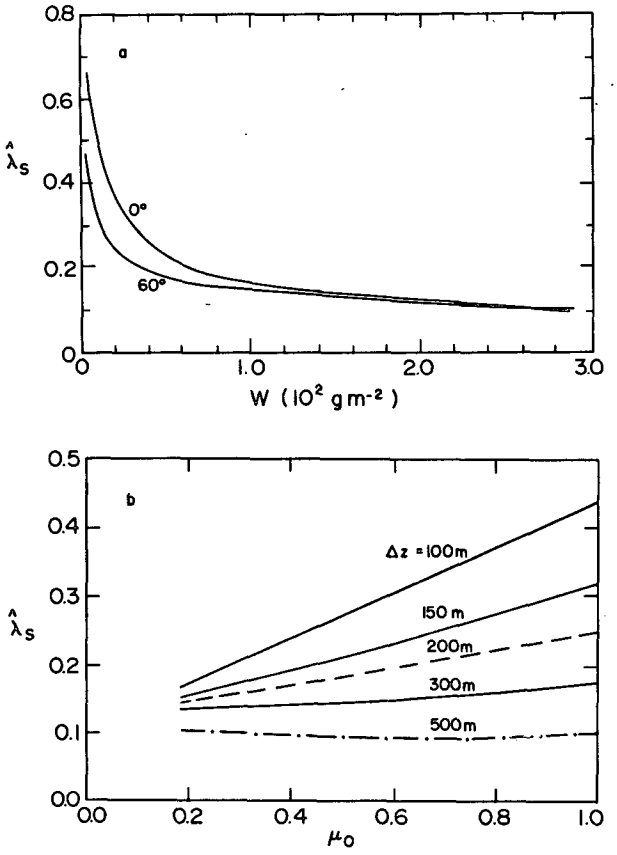

FIG. 3. Nondimensionalized solar decay scales, from ATRAD, as functions of (a) cloud LWC and (b) μ_0. The cutoff in (b) corresponds to the lowest value of μ_0 used, equivalent to a zenith angle of 80°.

Our interest is in the behavior of the physical decay scales, $\lambda_s = (z_B - z_C)\hat{\lambda}_s$ as a function of cloud LWC, which is shown in Fig. 4 (solid curves). The dashed curves in Fig. 4 are taken from the function

$$\lambda_s = a(\mu_0)W + b(\mu_0)\{1 - \exp[-(\gamma W + c(\mu_0))]\}, \quad (3.5)$$

where W is expressed in g m^{-2}, $\gamma = 0.021$ and

$$a(\mu_0) = -0.022 + 0.038(1 - \mu_0), \quad (3.6a)$$

$$b(\mu_0) = 56.8 - 14.7(1 - \mu_0), \quad (3.6b)$$

$$c(\mu_0) = 1.07 - 1.15(1 - \mu_0). \quad (3.6c)$$

By rearranging (3.2)–(3.4), we can now write the parameterized solar flux profile within the cloud as

$$F(\hat{z}) = F_B - \Delta F\{1 - \exp[-(1 - \hat{z})/\hat{\lambda}_s]\}/[1 - \exp(-1/\hat{\lambda}_s)], \quad (3.7)$$

with $\Delta F = F_B - F_C$, and where $\hat{\lambda}_s = \lambda_s/(z_B - z_C)$ with λ_s being given by Eqs. (3.5)–(3.6). Profiles of $f(\hat{z})$ using Eqs. (3.5) and (3.6) are shown as thin curves in Figs. 2a and 2b. Although the ATRAD results are not precisely exponential curves, the fit is quite close. To the extent that ATRAD calculates radiative flux profiles correctly, the parameterization is accurate.

The important feature captured by the parameterization—that the solar heating is confined mostly to the upper part of the cloud—has been discussed by Liou (1973) and others; it is also present in more detailed solar absorption calculations and observations (e.g., Schmetz et al., 1981). This feature was missing from an earlier parameterization used by Hanson and Gruber (1982). The increasing tendency of the absorption to occur within the upper part of the cloud as the cloud becomes thicker, as shown clearly in Fig. 2, exerts a strong influence on the cloud turbulence (Hanson, 1987).

It is of interest to compare the decay scales from ATRAD to those derived (using a method similar to that used below for IR fluxes) from the two-stream approximation, shown as the dotted curve in Fig. 4 (this was used in Hanson, 1987). The effect of multiple scattering in ATRAD confines the decay scales to a few tens of meters, while the single scattering of the two-stream method allows much larger decay scales.

The parameterization is summarized in appendix B.

4. Infrared radiation

While the solar fluxes can be normalized by using the downward flux at the cloud top, $F_{B\downarrow}$, and the bulk cloud optical properties, the various sources of thermal energy within the boundary layer complicate the picture for the IR parameterization. As before, it is necessary to assume that the downward flux at the cloud top, $G_{B\downarrow}$, is known—this is a boundary condition. Although the emissivity of clouds is effectively unity for water contents greater than about 25 g m^{-2} (Stephens, 1978b), equivalent to a 150 m thick cloud in the present model, here we allow for partially emitting clouds in order to include thinner clouds in the parameterization. We begin by defining the black-body fluxes B:

$$\tilde{B}(z) = \sigma T(z)^4, \quad (4.1)$$

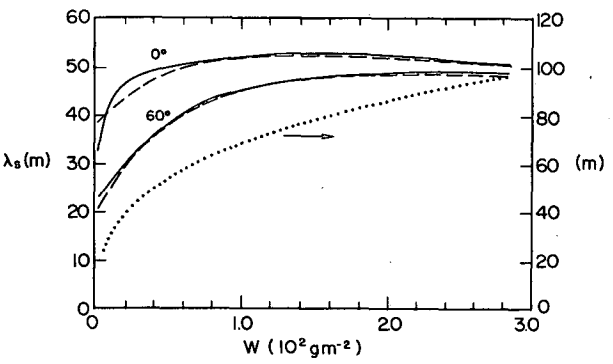

FIG. 4. Solar decay scales from ATRAD (solid) and from Eqs. (3.5)–(3.6) (dashed) for two solar zenith angles. The dotted curve (corresponding to the right-hand scale) are decay scales derived from the two-stream approximation and used in Hanson (1987).

where σ is the Stephan-Boltzman constant and T is absolute temperature. The emissivities of the surface and subcloud layer are denoted as ϵ_S and ϵ_{SC}, respectively; in general, ϵ_{SC} will differ for upward and downward fluxes. (Here, we assume that it is known.) The cloud emissivity will be included here in following the "effective emissivity" approach (e.g., Cox, 1976; Stephens, 1978b); accordingly, the upward IR flux at various levels is

$$\tilde{G}\uparrow = \tilde{G}_C\uparrow(1-\epsilon\uparrow) + \epsilon\uparrow\tilde{B}, \tag{4.2a}$$

where

$$\tilde{G}_C\uparrow = \epsilon_S(1-\epsilon_{SC}\uparrow)\tilde{B}_S + \epsilon_{SC}\uparrow\tilde{B}_{SC} \tag{4.2b}$$

with $\tilde{B}_{SC}$ evaluated at an average subcloud temperature T_{SC}. The downward IR fluxes are

$$\tilde{G}\downarrow = \tilde{G}_B\downarrow(1-\epsilon\downarrow) + \epsilon\downarrow\tilde{B}, \tag{4.3a}$$

$$\tilde{G}_S\downarrow = \tilde{G}_C\downarrow(1-\epsilon_{SC}\downarrow) + \epsilon_{SC}\downarrow\tilde{B}_{SC}. \tag{4.3b}$$

Equations (4.2a) and (4.3a) are identical to Stephens' (1978b) Eqs. (14a, b) in the present notation; these forms are used for consistency with the emissivity parameterization developed in that paper:

$$\epsilon\uparrow\downarrow = 1-\exp(-\alpha\uparrow\downarrow W), \tag{4.4}$$

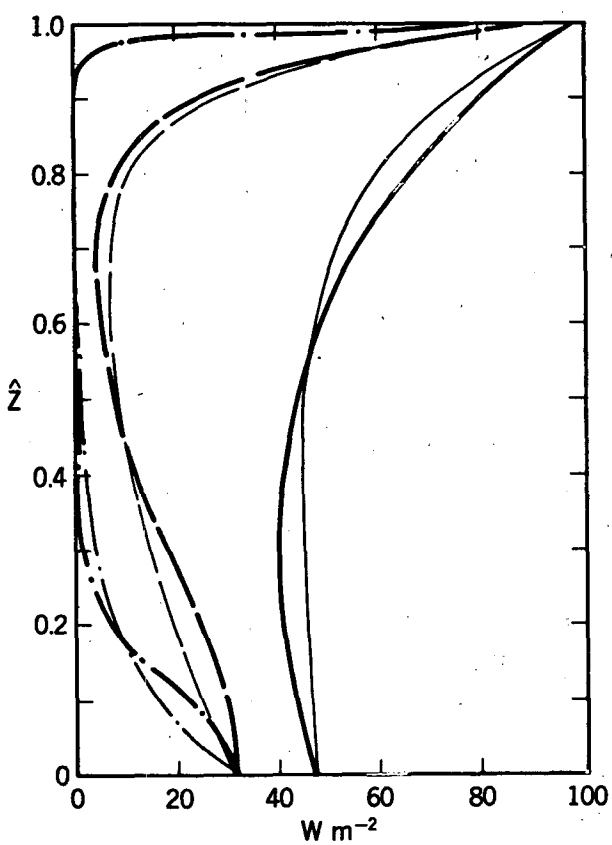

FIG. 5. IR fluxes vs nondimensional height from the emissivity method (heavy curves) and the parameterization (thin curves) for three different cloud thicknesses (as in Fig. 2a).

TABLE 1. Physical quantities specified for IR calculations.

Quantity	Symbol	Value
Cloud base height	z_C	400 m
Cloud base temperature	T_C	284 K
In-cloud temperature gradient	$-\beta g/C_p$	$-0.48g/C_p$ K m^{-1}
Upward cloud base IR flux	$G_C\uparrow$	400 W m^{-2}
Downward cloud top IR flux	$G_B\downarrow$	275 W m^{-2}

where $\alpha\uparrow\downarrow$ = (0.130; 0.158) and W is in g m^{-2}. This formula verifies quite well against a detailed numerical radiative transfer model used to simulate nocturnal stratocumulus observations (Slingo et al., 1982a).

The cloud liquid water contents below and above nondimensional level $\hat{z} \equiv (z-z_C)/(z_B-z_C)$ within the idealized layer cloud described in section 2a are

$$W_L = W\hat{z}^2 \tag{4.5a}$$

$$W_U = W(1-\hat{z}^2), \tag{4.5b}$$

where W is the total LWC from Eq. (2.1). Defining nondimensional factors

$$\eta\uparrow,\downarrow \equiv \alpha\uparrow,\downarrow W \tag{4.6}$$

allows the effective emissivities to be written as

$$\epsilon\uparrow = 1-\exp(-\eta\uparrow\hat{z}^2), \tag{4.7a}$$

$$\epsilon\downarrow = 1-\exp[\eta\downarrow(1-\hat{z}^2)]. \tag{4.7b}$$

Since the temperature variation through the cloud is relatively small, even for thick clouds, the black-body flux dependence can be linearized with virtually no loss of accuracy:

$$\tilde{B}(\hat{z}) = \tilde{B}_C(1-\hat{z}) + \tilde{B}_B\hat{z}, \tag{4.8}$$

and the net flux by the effective emissivity method is

$$\begin{aligned}\tilde{G}(\hat{z}) = {} & (\tilde{G}_C\uparrow - \tilde{B}_C)\exp(-\eta\uparrow\hat{z}^2) \\ & + (\tilde{B}_B - \tilde{G}_B\downarrow)\exp[-\eta\downarrow(1-\hat{z}^2)] - (\tilde{B}_B - \tilde{B}_C) \\ & \times\{(1-\hat{z})\exp[-\eta\downarrow(1-\hat{z}^2)] - \hat{z}\exp(-\eta\uparrow\hat{z}^2)\}.\end{aligned} \tag{4.9}$$

Figure 5 shows the net IR flux profiles (heavy curves) from (4.9) for clouds of various thickness. (Other parameters are given in Table 1.) Two significant aspects of these profiles complicate the parameterization developed later. First, the increase of liquid water with height causes very different decay scales at cloud top and cloud base. Second, thin clouds (e.g., the 100-m cloud) are so far from black that the net IR flux is nonzero everywhere within the cloud. Both of these factors are present in observations (e.g., Slingo et al., 1982a).

While (4.9) is analytic in $\hat{z}^2$, its integrals, which are needed in cloud modeling, are rather cumbersome. Also, in the limit of thick clouds, the third term contributes little to the flux. Because the exponential decay

approach used for the solar flux was so successful, and because it allows straightforward interpretation of the interaction of the radiative heating and turbulence in the cloud (Hanson, 1987), we are motivated to seek an analogous parameterization for the IR flux.

Accordingly, we seek a parameterization such that (4.9) is approximated as

$$G(\hat{z}) = G_L \exp(-\hat{z}/\hat{\lambda}_L) + G_U \exp(-(1-\hat{z})/\hat{\lambda}_U), \quad (4.10)$$

where the decay scales are nondimensionalized as $\hat{\lambda}_{L,U} = \lambda_{L,U}/(z_B - z_C)$. We thus require conditions to find the four unknowns $G_{L,U}$ and $\hat{\lambda}_{L,U}$.

To accomplish this we split the IR flux into contributions associated with the cloud top and base and match the vertical integrals of $\tilde{G}$ and G from each contribution. In physical terms, this ensures that the effect of the parameterized fluxes on the turbulence budget of the cloud matches that of the fluxes from the emissivity method. In terms of contributions from above and below (see appendix A for symbol definitions) these integrals can be written as

$$\tilde{G}_L \Lambda\uparrow = G_L \hat{\lambda}_L [1 - \exp(-1/\hat{\lambda}_L)], \quad (4.11)$$

$$\tilde{G}_U \Lambda\downarrow = G_U \hat{\lambda}_U [1 - \exp(-1/\hat{\lambda}_U)]. \quad (4.12)$$

The left sides, the integrals of the components of $\tilde{G}$, involve the integrals of $\exp(-\eta\uparrow\hat{z}^2)$ and $\exp[-\eta\downarrow(1 - \hat{z}^2)]$.

The other two conditions needed to find the four unknowns in (4.10) equate the fluxes at the cloud base and top:

$$\tilde{G}(\hat{z}=0) = G_L + G_U \exp(-1/\hat{\lambda}_U), \quad (4.13a)$$

$$\tilde{G}(\hat{z}=1) = G_L \exp(-1/\hat{\lambda}_L) + G_U. \quad (4.13b)$$

Equations (4.11–4.13) can be reduced to one algebraic equation in $(1/\hat{\lambda}_L)$ that can be solved iteratively. The resulting values of $\lambda_{U,L}$ can be approximated using analytic functions of the forms

$$\lambda_U = a_U W^{b_U}, \quad (4.14a)$$

with $a_U = 140.0$, $b_U = -0.56$ (and W in g m^{-2} as before), and

$$\lambda_L = a_L \chi^2 / [\chi(\chi - 1) + b_L], \quad (4.14b)$$

where $\chi = W^{0.5}$, $a_L = 70$ and $b_L = 2.67$ with similar unitary conventions to those for λ_U. Figure 6 shows these functions (dashed) and the original values of $\lambda_{U,L}$ derived from the emissivity method. The dependence of λ_L on W is particularly difficult to mimic, but the form of (4.14b) is reasonably close. The sensitivity of λ_U and λ_L to the various specified parameters (Table 1) is low, on the order of 5% for physically reasonable changes in T_C, $G_C\uparrow$ and $G_B\downarrow$. The fit of (4.14b) to the original calculations is well within this variability.

The complete IR parameterization is summarized in appendix B and, as mentioned, is considerably more complicated than the solar flux parameterization. The

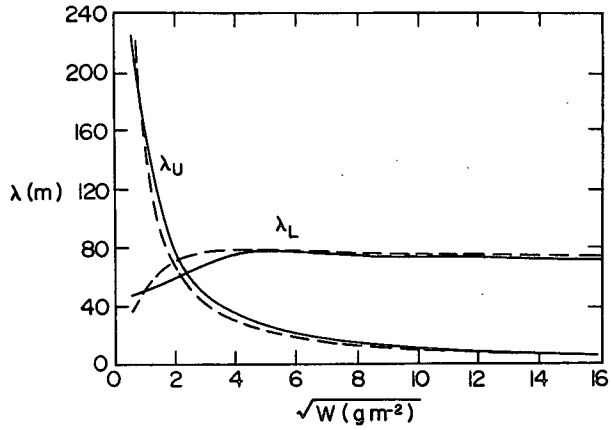

FIG. 6. IR decay scales from the emissivity method (solid) and Eqs. (4.14a, b) (dashed). The square root scale on the abscissa is used to accentuate the behavior at low LWC and is proportional to cloud thickness.

results are presented in Fig. 5 as the thin curves. In general, the parameterization works quite well, with flux errors less than about 7 W m^{-2}. Thin clouds present the most problem, with the cloud top cooling being spread over a deeper layer by the parameterization than by the emissivity method. Note that for the thickest of the three clouds used here (500 m), the cooling is confined to within about 50 m of cloud top, while the cooling extends over about the top 60 m of the 200 m thick cloud. This has important implications for the turbulence generation processes, as discussed in Hanson (1987).

Because the IR parameterization deviates from the more physical calculations of the emissivity method rather more than did the solar parameterization from ATRAD, we are motivated to compare IR fluxes from the parameterization with observations and numerical calculations. For this purpose, we use data and numerical model results from the Joint Air–Sea Interaction Experiment (JASIN) reported by Slingo et al. (1982b), from aircraft flights in North Sea stratocumulus reported by Nicholls (1984) and from balloon measurements of nocturnal stratocumulus reported by Slingo et al. (1982a). The data include measurements of LWC, T_B, T_C, z_B, z_C and the radiative fluxes. The observed liquid water content profiles were nearly linear in these experiments. In the papers referred to, the numerical model of Roach and Slingo (1979) for IR fluxes was used to simulate the observations and we also include those results in our comparison. In the figures to follow, dotted lines represent the data, solid lines the numerical model results and dashed lines the parameterization.

The IR fluxes from JASIN and the North Sea stratocumulus are given in Figs. 7a and 7b. The discrepancy of the JASIN observations and numerical calculations has been discussed by Slingo et al. (1982b)

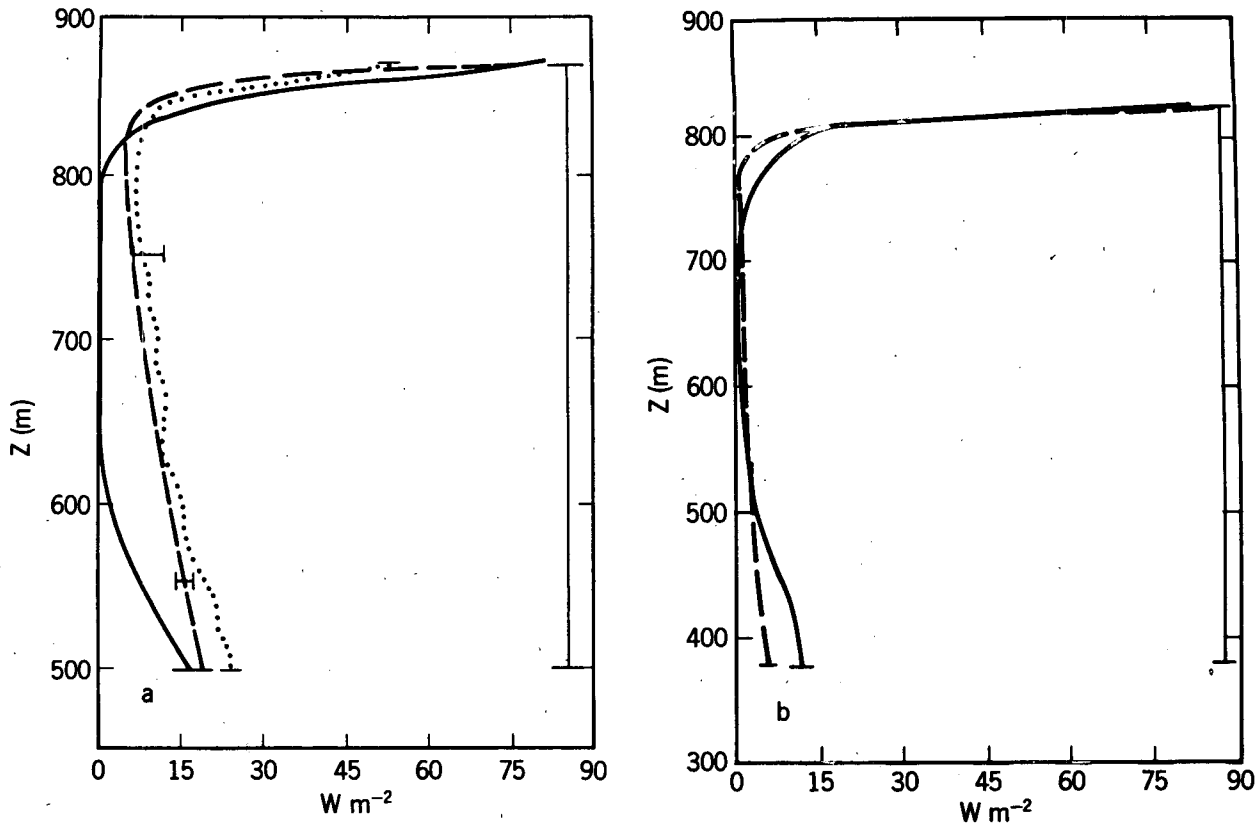

FIG. 7. Net upward IR flux comparison. (a) JASIN data (dotted line), numerical simulation (solid) and parameterization (dashed). (b) North Sea stratocumulus comparison, similar conventions (no data available). Cloud extent corresponds to vertical bar.

and attributed to measurement errors in cloud. That the parameterization reproduces the observations may be coincidental. The parameterization overpredicts the cloud top extinction, although the heating rates (not shown) are closer to the numerical calculations since the flux does not fall off as much. For the North Sea stratocumulus (Fig. 7b), the parameterization again overpredicts the abruptness of the cloud top flux decrease; this figure also shows an underprediction of the cloud base warming compared to the numerical model. (Net IR flux data were not available in this case, due to an instrument failure.)

Figure 8 shows more comparisons of IR fluxes, with the data this time taken from the nocturnal observations of Slingo et al. (1982a). Only net fluxes were reported in these cases, so that the test of the parameterization is limited to matching the cloud top and base fluxes and calculating the decay scales. The data and numerical computations have been replotted on nondimensional height coordinates from the original pressure coordinates; salient parameters are given in the insets. For the thinnest cloud (Fig. 8a), there is a range of LWCs that can be used (the liquid water profile was not exactly linear) and two extreme values are used in the parameterization. The lower value, 18 g m^{-2}, underpredicts the net flux in midcloud, and the larger value overpredicts the cloud top flux decrease as in the previous cases. The fluxes in Fig. 8b, within a somewhat thicker cloud, exhibit the same characteristics as the JASIN cloud, with the observations and numerical calculations showing less discrepancy. Finally, Fig. 8c shows fluxes in a very thick cloud, with the parameterization and numerical calculations showing close correspondence. In this case, the cloud top flux decreases from $\sim$80 W m^{-2} to virtually zero in 40 m.

These comparisons show that, while not precise, the IR parameterization developed in this paper give reasonable profile shapes for in-cloud IR fluxes. Differences in the IR fluxes are generally less than $\sim$5 W m^{-2}, if the profiles are adjusted vertically to more nearly match. The cloud-integrated heating predicted by the parameterization matches that of the emissivity method (this was a constraint of the derivation). For use in simple cloud dynamical models, the forms given before are probably sufficient, pending more precise IR flux measurements and LWC data.

5. Conclusion

This paper has been concerned with developing simplified parameterizations for the shapes of radiative flux profiles within layer clouds. Climate modelers re-

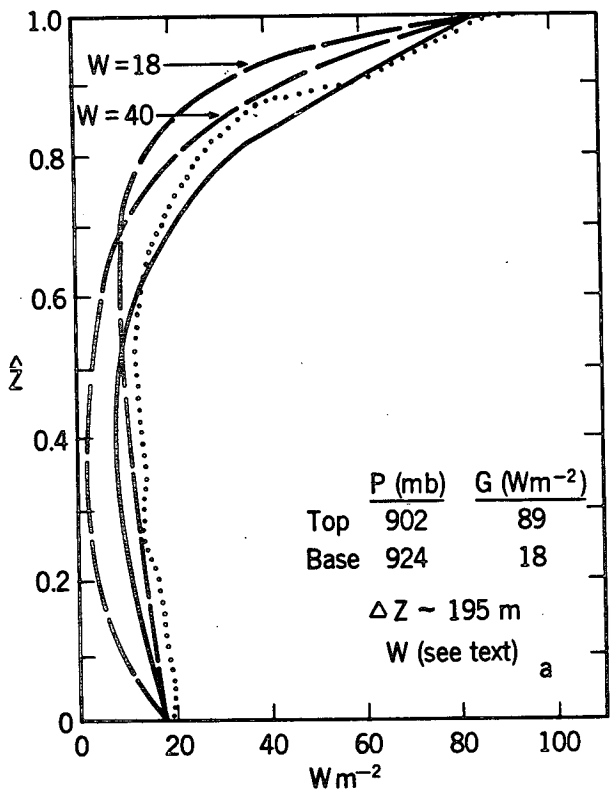

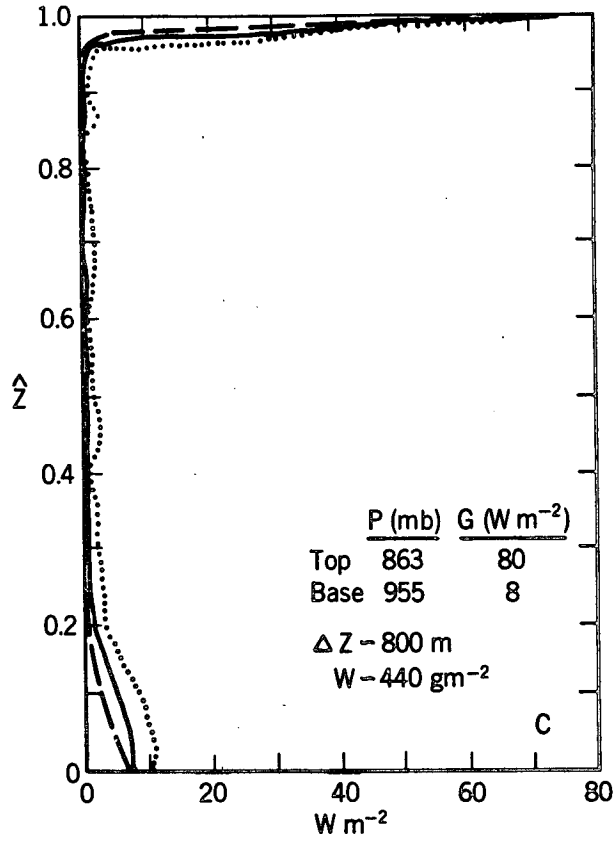

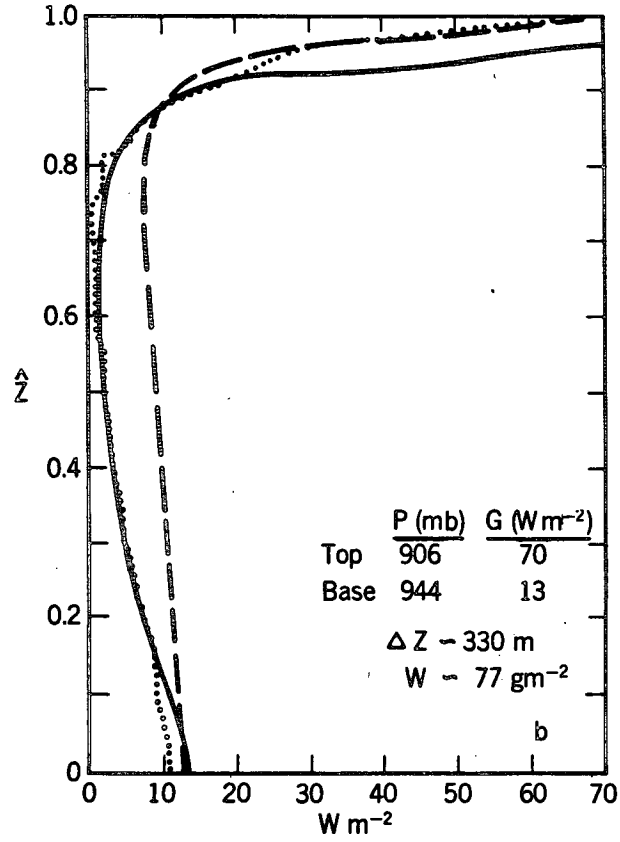

FIG. 8. An IR comparison for nocturnal stratocumulus, showing fluxes vs nondimensional height. Cloud thicknesses and LWCs noted in insets.

quire alternatives to numerical methods for radiative transfer computations, and the importance of clouds in climate underscores the need for simplified methods of cloud-radiation interaction calculations. The parameterizations developed here present one such simplification. They are based on the simplest possible physically realistic cloud model, a mixed layer model in which liquid water increases linearly with height. The general method used is applicable, however, to other distributions of cloud water.

The solar radiation parameterization relies on bulk cloud properties from other sources (e.g., Stephens, 1978b and Stephens et al., 1984 or Liou and Wittman, 1979) to derive the solar fluxes at cloud base and cloud top. The flux profile follows an exponential curve within the cloud, with a decay scale derived from numerical radiative transfer calculations based on the ATRAD narrow-band model (Wiscombe et al., 1984).

The IR radiation parameterization is based on constraints derived from the emissivity method (Cox, 1976) and uses a double exponential profile with different decay scales at the cloud base and cloud top. This is justifiable physically by the radically different cloud water contents near the two boundaries. Near cloud base, the liquid water mixing ratio increases from zero with height, while near cloud top it can be quite large and decreases with decreasing height. The parameterization matches cloud top and base fluxes with the emissivity method, and further requires that the vertical flux integrals match.

The parameterizations, summarized in appendix B, are meant to apply only to horizontally homogenous, plane-parallel clouds, and for this purpose, they represent the shape of the solar and IR flux profiles within the clouds reasonably faithfully. Extension of this work to include more realistic cloud geometry and alternate microphysical properties remains for the future.

Acknowledgments. The first author has been supported in this research by National Science Foundation through Grant ATM 82-09115 and, in the latter stages, by the National Aeronautics and Space Administration through Research Grant NAG-1-651 and the Office of Naval Research through Contract N00014-84-K-0405. The data in Fig. 1 were obtained during a number of NOAA-sponsored field experiments. We thank Suchi Psarakos for managing those experiments and Don Hooper for programming assistance. We are particularly grateful to Dr. Warren J. Wiscombe, NASA/GSFC, for supplying us with the ATRAD code and documentation and with considerable constructive criticism and insight into this research.

APPENDIX A

Infrared Radiation Derivation

The IR parameterization derived here depends on the nature of the physically based solutions to the emissivity method that are used as constraints to find the unknowns in Eq. (4.10). This is because the integral constraint is separated into the "upper" and "lower" contributions. Here, the appropriate definitions for Eqs. (4.11)–(4.13) are presented.

The net IR fluxes from the emissivity method at cloud base and cloud top *in the thick cloud limit* are

$$\left.\begin{aligned}\tilde{G}_L &\equiv \tilde{G}_C\uparrow - \tilde{B}_C\\ \tilde{G}_U &\equiv \tilde{B}_B - \tilde{G}_B\end{aligned}\right\}. \tag{A1}$$

Correction factors for the $(\tilde{B}_B - \tilde{B}_C)$ terms in Eq. (4.9) are defined as

$$\left.\begin{aligned}\xi\uparrow &\equiv 1 + (\tilde{B}_B - \tilde{B}_C)/(\tilde{G}_C\uparrow - \tilde{B}_C)\\ \xi\downarrow &\equiv 1 - (\tilde{B}_B - \tilde{B}_C)/(\tilde{B}_B - \tilde{G}_B\downarrow)\end{aligned}\right\}. \tag{A2}$$

The vertical integrals of the components of $\tilde{G}$ can be accounted for by defining

$$\left.\begin{aligned}\Lambda\uparrow &\equiv \xi\uparrow \int_0^1 \exp[-\eta\uparrow\hat{z}^2]d\hat{z}\\ &\qquad -(1-\xi\uparrow)[1-\exp(-\eta\uparrow)]/(2\eta\uparrow)\\ \Lambda\downarrow &\equiv \xi\downarrow \int_0^1 \exp[-\eta\downarrow(1-\hat{z}^2)]d\hat{z}\\ &\qquad +(1-\xi\downarrow)[1-\exp(\eta\downarrow)]/(2\eta\downarrow)\end{aligned}\right\}. \tag{A3}$$

This leads to (4.11) and (4.12).

APPENDIX B

Algorithm

The solar and IR parameterizations are summarized here. They rely on values of several quantities as external conditions. These include z_B, z_C, W, T_B, T_C, $F_B\downarrow$, μ_0, $G_C\uparrow$, $G_B\downarrow$, $\alpha\uparrow$ (=0.13), and $\alpha\downarrow$ (=0.158). For the solar flux calculation, it is first necessary to use the parameterization of Stephens et al. (1984) (or some other suitable method) to find R_{net} and Ac_{net}. Then with W in g m^{-2} and with $\gamma = 0.021$

$$a(\mu_0) = -0.022 + 0.038(1-\mu_0),$$

$$b(\mu_0) = 56.8 - 14.7(1-\mu_0),$$

$$c(\mu_0) = 1.07 - 1.15(1-\mu_0).$$

$$\lambda_s = a(\mu_0)W + b(\mu_0)(1-\exp\{-[\gamma W + c(\mu_0)]\}),$$

$$F_C = F_B + Ac_{\text{net}}F_B\downarrow,$$

$$F(z) = F_B - (F_B - F_C)[1-\exp(-(z_B-z)/\lambda_s)]/\{1-\exp[-(z_B-z_C)/\lambda_s]\}.$$

For the IR flux parameterization,

$$\lambda_U = 140.0W^{-0.56},$$

$$\lambda_L = 70.W/(W - W^{1/2} + 2.67),$$

$$B_B = \sigma T_B^4,$$

$$B_C = \sigma T_C^4,$$

$$\eta\uparrow,\downarrow \equiv \alpha\uparrow,\downarrow W,$$

$$\hat{G}_0 \equiv G_C\uparrow - B_C + (B_C - G_B\downarrow)\exp(-\eta\downarrow),$$

$$\hat{G}_1 \equiv (G_C\uparrow + B_B - 2B_C)\exp(-\eta\uparrow) + B_B - G_B\downarrow,$$

$$1/\lambda_N \equiv 1/\lambda_U + 1/\lambda_L,$$

$$\hat{D} \equiv 1 - \exp(-(z_B - z_C)/\lambda_N),$$

$$G_U = \{\hat{G}_1 - \hat{G}_0 \exp[-(z_B - z_C)/\lambda_L]\}/\hat{D},$$

$$G_L = \{\hat{G}_0 - \hat{G}_1 \exp[-(z_B - z_C)/\lambda_U]\}/\hat{D},$$

$$G(z) = G_L \exp[-(z - z_C)/\lambda_L] + G_U \exp[-(z_B - z)/\lambda_U].$$

REFERENCES

Albrecht, B. A., A. K. Betts, W. H. Schubert and S. K. Cox, 1979: A model of the structure of the trade-wind boundary-layer. Part I: Theoretical formulation and sensitivity tests. *J. Atmos. Sci.*, **36,** 73–89.

Betts, A. K., 1975: Parametric interpretation of trade-wind cumulus budget studies. *J. Atmos. Sci.*, **32,** 1934–1945.

Bretherton, F. P., V. E. Suomi, R. D. Cess, J. A. Coakley, S. K. Cox and D. A. Randall, 1983: FIRE (First International Satellite Cloud Climatology Project Regional Experiment) Research Plan. National Climate Research Program, Washington, DC, 76 pp.

Cox, S. K., 1976: Observation of cloud infrared effective emissivity. *J. Atmos. Sci.*, **33,** 287–289.

Deardorff, J. W., 1976: On the entrainment rate of a stratocumulus-topped mixed layer. *Quart. J. Roy. Meteor. Soc.*, **102,** 563–582.

——, 1981: On the distribution of mean radiative cooling at the top of a stratocumulus-capped mixed layer. *Quart. J. Roy. Meteor. Soc.*, **107,** 191–202.

Derr, V. E., and H. P. Hanson, 1984: Experimental optical and microphysical properties of clouds pertinent to radiative transfer. *IRS '84: Current Problems in Atmospheric Radiation,* G. Fiocco, Ed., A. Deepak Publishing Inc., 167–170.

Fravalo, C., Y. Fouquart and R. Rosset, 1981: The sensitivity of a model of low stratiform clouds to radiation. *J. Atmos. Sci.*, **38,** 1049–1062.

Hanson, H. P., 1984: Stratocumulus instability reconsidered: A search for physical mechanisms. *Tellus,* **36,** 355–368.

——, 1987: Radiative/turbulent transfer interactions in layer clouds. *J. Atmos. Sci.*, **44,** 1288–1295.

——, and P. L. Gruber, 1982: Effect of marine stratocumulus clouds on the ocean-surface heat budget. *J. Atmos. Sci.*, **39,** 897–908.

Kahn, P. H., and J. A. Businger, 1979: The effect of radiative flux divergence on the entrainment of a saturated convective boundary layer. *Quart. J. Roy. Meteor. Soc.*, **105,** 303–306.

Lilly, D. K., 1968: Models of cloud-topped mixed layers under a strong inversion. *Quart. J. Roy. Meteor. Soc.*, **94,** 292–309.

——, and W. H. Schubert, 1980: The effects of radiative cooling in a cloud-topped mixed layer. *J. Atmos. Sci.*, **37,** 482–487.

Liou, K.-N., 1973: A numerical experiment on Chandrasekar's discrete ordinate method for radiative transfer: Applications to cloud and hazy atmospheres. *J. Atmos. Sci.*, **30,** 1303–1326.

——, and G. D. Wittman, 1979: Parameterization of the radiative properties of clouds. *J. Atmos. Sci.*, **36,** 1261–1273.

Nicholls, S., 1984: The dynamics of stratocumulus: Aircraft observations and comparisons with a mixed layer model. *Quart. J. Roy. Meteor. Soc.*, **110,** 783–820.

Oliver, D. A., W. S. Lewellen and G. G. Williamson, 1978: The interaction between turbulent and radiative transport in the development of fog and low-level stratus. *J. Atmos. Sci.*, **35,** 301–316.

Randall, D. A., 1980a: Conditional stability of the first kind upside-down. *J. Atmos. Sci.*, **37,** 125–130.

——, 1980b: Entrainment into a stratocumulus layer with distributed radiative cooling. *J. Atmos. Sci.*, **37,** 148–159.

——, J. A. Coakley, C. W. Fairall, R. A. Kropfli and D. H. Lenschow, 1984: Outlook for research on subtropical marine stratiform clouds. *Bull. Amer. Meteor. Soc.*, **65,** 1290–1301.

Roach, W. T., and A. Slingo, 1979: A high resolution infrared radiative transfer scheme to study the interaction of radiation with cloud. *Quart. J. Roy. Meteor. Soc.*, **105,** 603–614.

Rogers, D. P., J. A. Businger and H. Charnock, 1985: A numerical investigation of the JASIN atmospheric boundary layer. *Bound.-Layer Meteor.*, **32,** 373–399.

Schmetz, J., E. Raschke and J. Fimpel, 1981: Solar and thermal radiation in maritime stratocumulus clouds. *Contrib. Atmos. Phys.*, **54,** 442–452.

Schneider, S. H., and R. E. Dickinson, 1976: Parameterization of fractional cloud amounts in climatic models: The importance of modeling multiple reflections. *J. Appl. Meteor.*, **15,** 1050–1056.

Schubert, W. H., J. S. Wakefield, E. J. Steiner and S. K. Cox, 1979a: Marine stratocumulus convection. Part I: Governing equations and horizontally homogeneous solutions. *J. Atmos. Sci.*, **36,** 1286–1307.

Slingo, A., R. Brown and C. L. Wrench, 1982a: A field study of nocturnal stratocumulus: III. High resolution radiative and microphysical observations. *Quart. J. Roy. Meteor. Soc.*, **108,** 145–166.

——, S. Nicholls and J. Schmetz, 1982b: Aircraft observations of marine stratocumulus during JASIN. *Quart. J. Roy. Meteor. Soc.*, **108,** 833–856.

Stephens, G. A., 1978a: Radiation profiles in extended water clouds. Part I: Theory. *J. Atmos. Sci.*, **35,** 2111–2122.

——, 1978b: Radiation profiles in extended water clouds. Part II: Parameterization. *J. Atmos. Sci.*, **35,** 2123–2132.

——, 1984: The parameterization of radiation for numerical weather prediction and climate models. *Mon. Wea. Rev.*, **112,** 826–867.

——, G. W. Paltridge and C. M. R. Platt, 1978: Radiation profiles in extended water clouds. Part III: Observations. *J. Atmos. Sci.*, **35,** 2133–2141.

——, S. Ackerman and E. A. Smith, 1984: A shortwave parameterization revised to improve cloud absorption. *J. Atmos. Sci.*, **41,** 687–690.

Welch, R. M., and B. A. Wielicki, 1985: A radiative parameterization of stratocumulus cloud fields. *J. Atmos. Sci.*, **42,** 2888–2897.

Wiscombe, W. J., and R. Welch, 1986: Reply [to Hegg]. *J. Atmos. Sci.*, **43,** 401–407.

——, R. M. Welch and W. D. Hall, 1984: The effects of very large drops on cloud absorption. Part I: Parcel models. *J. Atmos. Sci.*, **41,** 1336–1355.